Optical phonons and the soft mode in $2H$-$NbSe_2$

F. Weber,[1] R. Hott,[1] R. Heid,[1] K.-P. Bohnen,[1] S. Rosenkranz,[2] J.-P. Castellan,[2] R. Osborn,[2] A. H. Said,[3] B. M. Leu,[3] and D. Reznik[4]

[1]*Institute of Solid State Physics, Karlsruhe Institute of Technology, 76021 Karlsruhe, Germany*
[2]*Materials Science Division, Argonne National Laboratory, Argonne, Illinois 60439, USA*
[3]*Advanced Photon Source, Argonne National Laboratory, Argonne, Illinois 60439, USA*
[4]*Department of Physics, University of Colorado at Boulder, Boulder, Colorado 80309, USA*

(Received 12 November 2012; revised manuscript received 15 April 2013; published 17 June 2013)

We present an investigation of the lattice dynamics of the charge density wave (CDW) compound $2H$-$NbSe_2$. We analyze the precise nature of the wave vector-dependent electron-phonon coupling (EPC) and derive the bare dispersion of the CDW soft phonon mode using inelastic x-ray scattering combined with *ab initio* calculations. Experimentally, phonon modes along the $\Gamma - M$ line, i.e., $\mathbf{q} = (h,0,0)$, with $0 \leqslant h \leqslant 0.5$ and the same longitudinal symmetry (Σ_1) as the CDW soft mode, were investigated up to 32 meV. In agreement with our calculations, we observe significant EPC in the optic modes at $h \leqslant 0.2$. We analyze the EPC in the optic, as well as acoustic, mode and show that the $\mathbf{q}$ dependences stem from scattering processes between two bands at the Fermi surface that both have a Nb $4d$ character. Finally, we demonstrate that the soft mode dispersion at $T = 33$ K ($=T_{\mathrm{CDW}}$) can be well described on the basis of a strongly $\mathbf{q}$-dependent EPC matrix element and an acousticlike bare phonon dispersion in agreement with observations near room temperature.

DOI: 10.1103/PhysRevB.87.245111 PACS number(s): 71.45.Lr, 63.20.kd, 63.20.dd, 63.20.dk

I. INTRODUCTION

Charge density wave (CDW) formation is one of the most common phenomena in solid state physics and relevant to a number of important issues in condensed matter physics, such as the role of stripes in cuprate superconductivity[1] and charge fluctuations in the colossal magnetoresistive manganites.[2] Static CDW order, i.e., a periodic modulation of the electronic density, can only be stabilized in case of a nonzero electron-phonon coupling (EPC), specifically, coupling of phonons to electrons in the conduction bands. Hence, the electronic modulation is accompanied by a lattice distortion involving a soft phonon mode with a zero energy at $\mathbf{q} = \mathbf{q}_{\mathrm{CDW}}$ and $T = T_{\mathrm{CDW}}$.

$2H$-$NbSe_2$ is a prototypical CDW compound. It was originally investigated more than four decades ago as one of the first layered materials in which superconductivity was observed (T_{SC} ($2H$-$NbSe_2$) = 7.2 K).[3] Only afterward was it realized that $2H$-$NbSe_2$ undergoes a CDW phase transition at $T_{\mathrm{CDW}} = 33$ K,[4] although the exact distortion pattern at $T < T_{\mathrm{CDW}}$ is still a subject of research.[5] Original ideas on the origin of the CDW formation centered on the Fermi surface nesting; however, subsequent experiments found that CDW in some compounds appears without strong Fermi surface nesting.[6] An early alternative mechanism based on a $\mathbf{q}$-dependent enhancement of the EPC matrix element g_q has been proposed. A prominent role of EPC and, in particular, the wave vector dependence of g_q have been suggested.[7–9] Experimentally, however, the small size of $2H$-$NbSe_2$ single crystals allowed only a limited investigation of the CDW soft phonon mode close to T_{CDW} by inelastic neutron scattering.[10–12] Earlier, we reported high-resolution inelastic x-ray scattering experiments showing evidence that in $2H$-$NbSe_2$, the wave vector dependence of g_q is at the origin of the CDW transition.[13]

Any realistic model of soft phonons in CDW compounds must begin with understanding of the bare phonon dispersion $\omega_{\mathrm{bare}}(q)$, which is the dispersion without the interaction of the phonon with electrons in the conduction bands. It takes into account the screening of the ionic movements by the strongly bound core electrons but not the more subtle effects due to electronic scattering processes near the Fermi surface. Extracting $\omega_{\mathrm{bare}}(q)$ is not a trivial task, because it cannot be measured directly. Furthermore, it is necessary to go beyond the simple assumption that the soft phonon must derive from an acoustic branch, because optic phonons can also soften to zero energy if they are coupled to conduction electrons strongly enough.

In this paper, we derive the bare phonon dispersion $\omega_{\mathrm{bare}}(q)$ of the CDW soft mode in $NbSe_2$ from a detailed analysis of the wave vector-dependent EPC, the correlated electronic scattering processes, and the phonon displacement patterns. Because the soft phonon mode is not necessarily acousticlike, optic phonons of the same symmetry as the soft mode had to be investigated as well. We have measured phonons with Σ_1 symmetry up to 32 meV, providing evidence of EPC in the optical branches at small wave vectors. These results are in good agreement with our *ab initio* calculations, and we used the latter to further analyze the observed EPC in the optic, as well as acoustic, phonons. We found that the wave vector dependence of EPC in the investigated phonons is primarily due to electronic scattering processes between two Nb $4d$-derived bands at the Fermi surface. Furthermore, the phonon patterns do not indicate an exchange of eigenvectors between optic and acoustic phonons. Accordingly, the soft mode at $T = T_{\mathrm{CDW}}$ is acousticlike.

II. THEORY

Calculations using density functional perturbation theory (DFPT) were performed in the framework of the mixed-basis pseudopotential method.[14] The exchange-correlation functional was treated in the local-density approximation. Norm-conserving pseudopotentials for Nb and Se were constructed, including $4s$ and $4p$ semicore states in the valence space in the

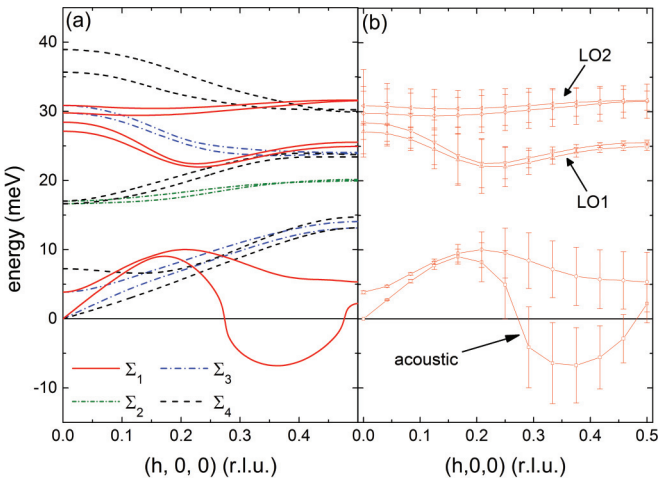

FIG. 1. (Color online) (a) Calculated phonon dispersion along the (100) direction in $NbSe_2$. Different line types (colors) denote branches with different symmetries (see legend). (b) Branches with longitudinal symmetry (Σ_1) [solid lines in (a)]. Labels correspond to the discussion. Vertical bars denote the calculated electronic contribution to the phonon line width 2γ, scaled by a factor of 10 for visibility.

case of Nb. The deep potentials can be efficiently treated in the mixed-basis scheme, which combines local functions and plane waves for the representation of the valence states. Local functions of s, p, and d symmetry at the Nb sites and of s and p symmetry on the Se sites were combined with plane waves up to 24 Ry.

Phonon energies and EPC were calculated using DFPT or the linear response technique,[15] in combination with the mixed-basis pseudopotential method.[16] To resolve fine features related to the Fermi surface geometry, Brillouin zone (BZ) integrations were performed with a dense hexagonal $24 \times 24 \times 8$ **k**-point mesh (244 points in the irreducible BZ). The standard smearing technique was employed with a Gaussian broadening of 0.1 eV. Tests with the denser **k**-point mesh confirmed sufficient convergence for both phonon energies and line widths. All results were obtained for the fully optimized hexagonal structure ($a = b = 3.40$ Å, $c = 12.09$ Å).

Imaginary phonon energies, shown as the negative roots of the square phonon energies in Fig. 1, appear in the calculation because of an anharmonic double-well potential reflecting the CDW instability. At zero temperature, the lattice distorts into a CDW and sits in one of the minima. However, the calculation assumes that the lattice is undistorted, i.e., that it sits in the middle (i.e., local maximum) of the double-well potential. Negative curvature of the potential at atomic positions of the high-temperature structure is what gives an imaginary calculated energy for the phonon whose eigenvector is close to the CDW distortion.

III. EXPERIMENT

The inelastic x-ray scattering experiments were carried out at the XOR 30-ID (HERIX) beamline of the Advanced Photon Source, Argonne National Laboratory, with a focused beam size of 30 μm. The incident energy was 23.724 keV (Ref. 17), and the horizontally scattered beam was analyzed by a set of spherically curved silicon analyzers (Reflection 12 12 12).[18] The full width at half maximum (FWHM) of the energy and wave vector space resolution was ~1.5 meV and 0.066 Å^{-1}, respectively, where the former is experimentally determined by scanning the elastic line of a piece of plastic and the latter is calculated from the experiment geometry and incident energy. The components (Q_h, Q_k, Q_l) of the scattering vector are expressed in reciprocal lattice units (r.l.u.) (Q_h, Q_k, $Q_l = h^*2\pi/a$, $k^*2\pi/a$, $l^*2\pi/c$) with the lattice constants $a = b = 3.443$ Å and $c = 12.55$ Å of the hexagonal unit cell, space group $P6_3/mmc$. Measurements were made in the constant-wave vector **Q** mode, i.e., as energy scans at constant wave vector $\mathbf{Q} = \boldsymbol{\tau} + \mathbf{q}$, where $\boldsymbol{\tau}$ is a reciprocal lattice point and **q** is the reduced wave vector. Measurements were done in the BZs adjacent to $\boldsymbol{\tau} = (3,0,0)$ and $(3,0,1)$, i.e., $\mathbf{Q} = (3-h,0,0)$ and $(3-h,0,1)$. We used a high-quality single crystal sample of ~50 mg ($2 \times 2 \times 0.05$ mm^3) with a T_{CDW} of 33 K determined from the temperature dependence of the superlattice reflections,[13] in agreement with previous results.[19] The sample was mounted in a closed-cycle refrigerator, and measurements reported here were done at various temperatures $33\ \mathrm{K} \leqslant T \leqslant 250\ \mathrm{K}$.

Measured energy spectra were fitted using a pseudo-Voigt function for the elastic line with a variable amplitude and fixed line shape established by scanning through the CDW superlattice peak at $T = 8$ K and reference scans of a piece of plastic. Phonon peaks were fitted by a damped harmonic oscillator (DHO) function[20]

$$S(Q,\omega) = \frac{[n(\omega)+1]Z(Q)4\omega\Gamma/\pi}{\left[\omega^2 - \tilde{\omega}_q^2\right]^2 + 4\omega^2\Gamma^2} \qquad (1)$$

where **Q** and ω are the wave vector and energy transfer, respectively; $n(\omega)$ is the Bose function; Γ is the imaginary part of the phonon self-energy; $\tilde{\omega}_q$ is the phonon energy renormalized by the real part of the phonon self-energy; and **Z**(**Q**) is the phonon structure factor. This function covers the energy loss and energy gain scattering by a single line shape and was convoluted with the experimental resolution. The intensity ratio of the phonon peaks at $E = \pm\omega_q$ is fixed by the principle of detailed balance. The energy ω_q of the damped phonons is obtained from the fit parameters of the DHO function by $\omega_q = \sqrt{\tilde{\omega}_q^2 - \Gamma^2}$ (Ref. 21). Here, $\tilde{\omega}_q$ is the phonon energy renormalized by the real part of the susceptibility, $Re\,\chi$, whereas ω_q is renormalized by both the real and the imaginary parts of the susceptibility.

IV. RESULTS

A. Density functional perturbation theory

Our calculated phonon dispersions are in good agreement with previous calculations.[22] In Fig. 1(a), we show the dispersion along the crystallographic (100) direction, including the CDW vector $\mathbf{q}_{\mathrm{CDW}} = (0.329,0,0)$.[19] Due to the double-layered structure within the hexagonal unit cell of $NbSe_2$, we observe pairs of branches with very small differences in absolute energy and dispersion except for the acoustic modes. As reported previously,[13] our calculations predict a broad range of wave vectors with imaginary phonon energies, indicating the structural instability. Nonetheless, we discuss our results

within the undistorted high-temperature structure, because we are interested in the lattice dynamics leading to the phase transition at and just above the phase transition.

Fig. 1(b) focuses on the longitudinal branches along the (100) direction that have Σ_1 symmetry. We also plot the momentum and energy-resolved calculated electronic contribution to the line width of the phonons, which is a direct measure of the EPC. Sizable contributions of EPC to the phonon line widths for the longitudinal acoustic (LA) and longitudinal optic (LO) phonon branches are calculated. In the two highest LO modes, we see little wave vector dependence of EPC, whereas the two LO branches starting at the zone center at 27.13 and 28.43 meV exhibit a clear decrease of EPC along the $\Gamma - M$ line [Fig. 1(b)]. Moreover, the EPC of the LA and lowest LO branches strongly increases in the wave vector range, where the line widths of the LO branches starting at 27.13 and 28.43 meV are reduced ($h = 0.2$–0.25 r.l.u.). The wave vectors where the dispersion of the LA mode has its maximum and the ones of the LO branches starting at 27.13 and 28.43 meV that have a minimum in their dispersions are in the same wave vector range $0.2 \leqslant h \leqslant 0.25$. Hence, an exchange of eigenvectors, which is possible for modes of the same symmetry, between the medium-energy LO modes and the LA branch cannot be excluded even though the energy gap is quite large (12–14 meV). Such an exchange of eigenvectors would change the discussion of the bare phonon energy in Sec. V. Instead of the softening of the LA branch, we would have to consider the softening of an LO phonon over more than 20 meV from the zone center to $\mathbf{q}_{\mathrm{CDW}}$.

For a more detailed analysis, and because both the experimental results for phonon energies and the line widths are in good agreement with the predictions of DFPT (see Sec. IV B), we looked into the calculated phonon eigenvectors of the three investigated modes, taking into account the respective electronic contributions to the phonon line width γ. The calculated absolute atomic displacements $\mathbf{u}_{\mathrm{atom}}$ for the LO1, LO2, and acoustic branches along the $\Gamma - M$ line are shown in Figs. 2(a)–2(c). In Figs. 2(d)–2(f), γs (half width at half maximum) of the three phonon branches are plotted. For the LO1 branch, the maximum in γ as a function of wave vector [Fig. 2(e)] coincides with the maximal Nb displacement $\mathbf{u}_{\mathrm{Nb}}$. In the acoustic branch, the strong maximum in γ at $h = 0.3$–0.35 [Fig. 2(f)] is accompanied by an increase of the corresponding $\mathbf{u}_{\mathrm{Nb}}$; however, it has only a very broad peak [Fig. 2(a)]. There is no clear correlation between the movements of the Se atoms [Figs. 2(b) and 2(c)] and the γ values. This indicates that the dominant part of γ is due to scattering by electronic states with a Nb character, as shown below. The LO2 branch does not show a relation between $\mathbf{u}_{\mathrm{Nb}}$ and γ, although there is a maximum in the former close to the zone center [Fig. 2(a)].

Here, it is instructive to look into the contributions to the total γ due to different scattering processes at the Fermi surface. Our calculated Fermi surface is produced by two Nb 4d-derived bands (which we call Nb_1 and Nb_2 for simplicity) and one band with a Se 4p character, in agreement with previous reports.[23,24] Apparently, electronic scattering paths between the two Nb 4d-derived bands are responsible for the strong maxima in the EPC of the LO1 and acoustic modes [Figs. 2(e) and 2(f)]. Furthermore, we see that the same scattering path yields a weak maximum in γ for the LO2

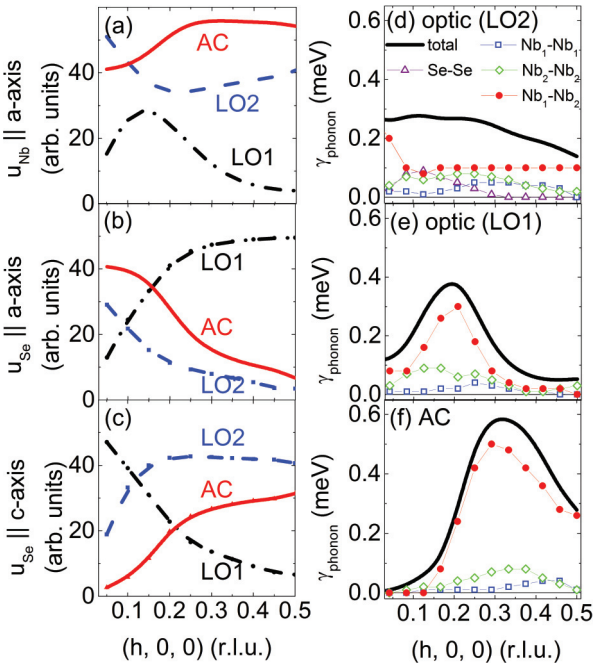

FIG. 2. (Color online) (a)–(c) The $\mathbf{q}$ dependence of the calculated absolute atomic displacements for the acoustic (AC), lower optic (LO1), and highest optic (LO2) branches. Three displacements are shown: (a) Nb $\parallel a$, (b) Se $\parallel a$, and (c) Se $\parallel c$. Other components are zero. (d)–(f) Calculated electronic contribution to the phonon line width γ for the (d) LO2, (e) LO1, and (f) AC branches. Each panel shows the total line width (solid line) and the dominant contributions related to specific electronic scattering processes.

branch close to the zone center [Fig. 2(d)], which coincides with the maximum in $\mathbf{u}_{\mathrm{Nb}}$ for this branch [Fig. 2(a)]. Hence, our analysis demonstrates that phonon displacements with strong Nb movements are necessary to produce a large and wave vector-dependent EPC. The consecutive maxima of γ in the LO2, LO1, and acoustic branches going from close to the zone center to the zone boundary, i.e., from $h = 0$ to 0.5, might indicate a certain transformation of a Nb character from the LO2 to the LO1 and then to the acoustic branch along this direction. However, the wave vector dependence of the Nb displacements, in particular the one of the acoustic branch, argues against a decisive role of such an exchange with respect to the formation of CDW order. $\mathbf{u}_{\mathrm{Nb}}$ increases by 1/3 at $h = 0.15$–0.35 and then is reduced by 3% farther toward the zone boundary [Fig. 2(a)]. However, the corresponding γ related to scattering between the Nb 4d-derived bands jumps from zero at a small wave vector to a clear maximum at $h = 0.3$ and then decreases again by 50% [red dots in Fig. 2(f)]. We conclude that DFPT does not predict an exchange of eigenvectors between the LO and the LA branches of Σ_1 symmetry in $NbSe_2$.

B. Experimental results

Experiments using inelastic neutron scattering to measure phonons in materials that have a CDW with good wave vector and energy resolution were limited to a small number of compounds, where sufficiently large single crystals could be grown.[25] Similar measurements in $NbSe_2$ gave only

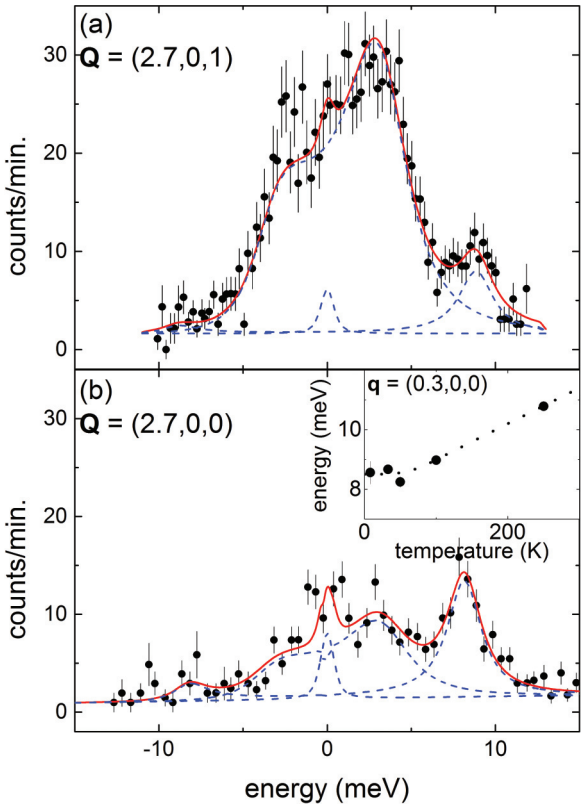

FIG. 3. (Color online) Raw inelastic x-ray scattering data obtained at $T = 50$ K and (a) $\mathbf{Q} = (2.7,0,1)$ and (b) $\mathbf{Q} = (2.7,0,0)$. Solid (red) lines are fits consisting of an elastic line, DHOs for the inelastic peaks, and a linear background shown as dashed (blue) lines. The inset in (b) shows the temperature-dependent phonon energy of the second-lowest longitudinal mode at $\mathbf{q} = (0.3,0,0)$. The dashed line is a visual guide.

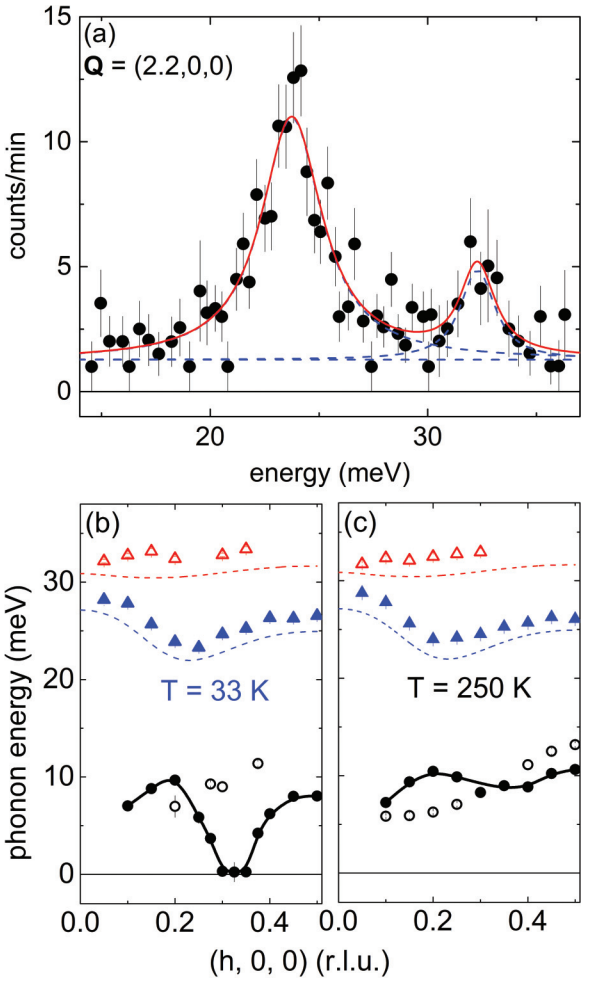

FIG. 4. (Color online) (a) Raw data showing two optic phonon modes at $\mathbf{Q} = (2.2,0,0)$ at $T = 33$ K. The solid (red) line is a fit consisting of two DHOs for the inelastic peaks convoluted with the experimental resolution and a linear background shown as dashed (blue) lines. Measured phonon dispersion is at (b) $T = 33$ K and (c) $T = 250$ K. Solid lines denote the dispersion associated with the soft phonon mode (see text), as published in Ref. 13. Dashed lines are the calculated energies of the LO1 and LO2 optic branches (see Fig. 1).

limited insight[10,11] into the dynamics in the pretransitional temperature region just above T_{CDW}. Apart from the small sample volume, previous measurements focused on the BZ adjacent to the reciprocal lattice vector $\boldsymbol{\tau} = (3,0,0)$. In contrast, our calculations predicted a much larger structure factor for the soft phonon mode around $\boldsymbol{\tau} = (3,0,1)$. Fig. 3 shows inelastic x-ray scattering raw data taken in the two BZs at a reduced wave vector of $\mathbf{q} = (0.3,0,0)$, which demonstrate the accuracy of the calculated structure factors and hence the calculated phonon pattern. The soft mode pattern includes movements of Se along the c axis, although the CDW-ordering wave vector has a zero component along the (001) direction.[10,19] Here, it is instructive to know that the eigenvector of the soft mode does not quantitatively reflect the structural distortion in the CDW-ordered phase. For instance, it is important to consider the superposition of the soft mode in different but equivalent directions, such as the three equivalent (100) directions in the hexagonal lattice of $2H$-$NbSe_2$. Extracting the CDW distortion from DFPT is possible in principle but outside the scope of this paper.

Energy scans of the optic phonon branches are shown in Fig. 4, along with the observed dispersion along the crystallographic (100) direction at $T = 33$ and 250 K. We measured the optic branches corresponding to the calculated ones starting at 27.13 meV (LO1) and 30.86 meV (LO2) at $\mathbf{Q} = (2+h,0,0)$. Scans in a different BZ showed phonon peaks at slightly higher and lower energies compared to the ones of LO1 and LO2 modes, respectively, in agreement with our structure factor calculations. Due to the limited amount of beam time, however, we could not determine all dispersions completely and focused on the branches detectable at $\mathbf{Q} = (2+h,0,0)$. In addition to the dispersion of the soft phonon reported earlier,[13] we include the phonon energies of the lowest LO branch with Σ_1 symmetry. The intensity ratio of the soft mode and this second-lowest energy branch is different in the two BZs adjacent to $\boldsymbol{\tau} = (3,0,0)$ and $(3,0,1)$ [Fig. 3], in agreement with DFPT. Therefore, an unambiguous assignment of the phonon characters of the soft mode and the lowest LO branch was possible in a simultaneous evaluation of energy scans at the same $\mathbf{q}$ value in the two BZs, i.e., adjacent to $\boldsymbol{\tau} = (3,0,1)$ and $(3,0,0)$. Apart from a small offset toward higher experimental energies, we see good agreement between the observed and the calculated phonon energies for the LO1 and LO2 branches. In

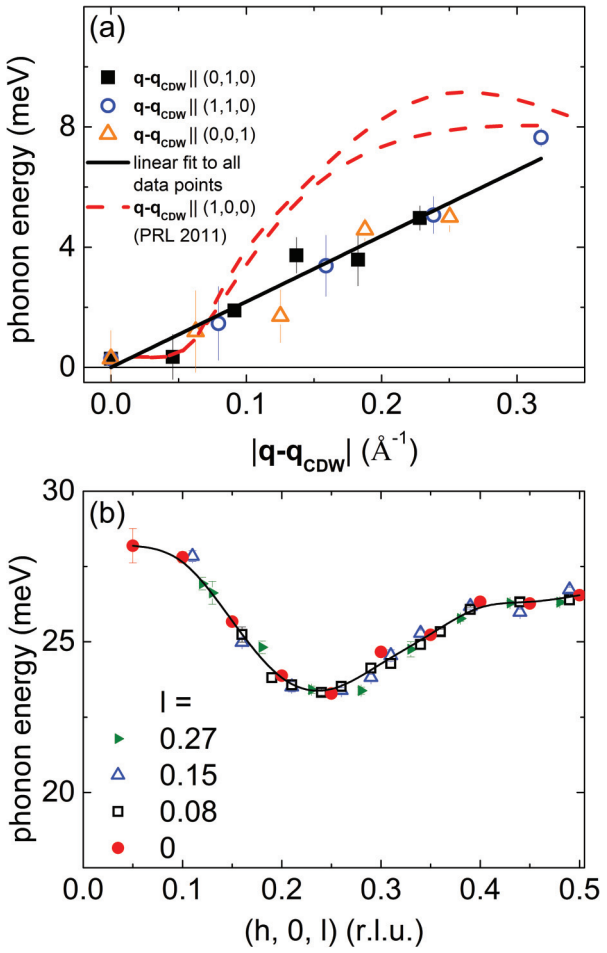

FIG. 5. (Color online) (a) Observed phonon energies at $T = 33$ K along a different high symmetry direction (different from [100]), starting from the CDW vector $\mathbf{q}_{CDW}$. Energies are shown as function of the distance from $\mathbf{q}_{CDW}$ in absolute units. The solid line is a linear fit of the data. The dashed lines indicate the corresponding phonon energies along the (100) direction, as published in (Ref. 4) (two lines for $\mathbf{q} < \mathbf{q}_{CDW}$ and $\mathbf{q} > \mathbf{q}_{CDW}$). (b) Dispersion of the LO1 branch at $T = 33$ K for different values of l along the [001] direction. The line is a visual guide.

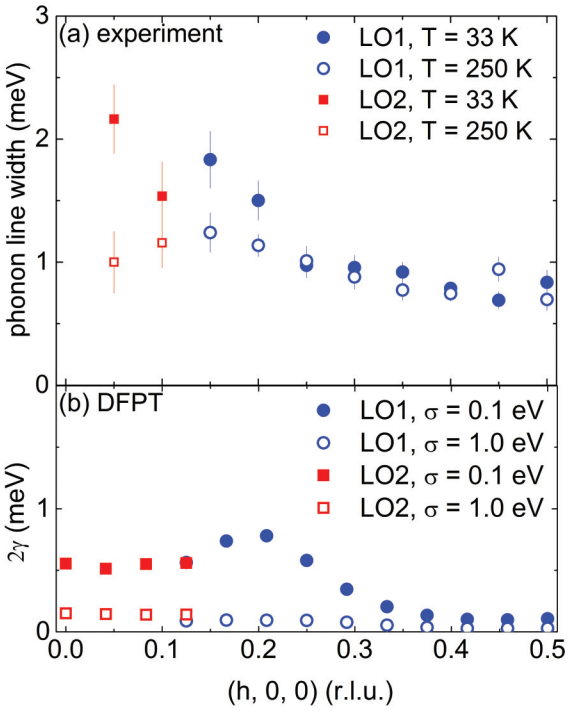

FIG. 6. (Color online) (a) Wave vector-dependent line widths (FWHM) at $T = 33$ K (filled symbols) and 250 K (open symbols) of the LO1 and LO2 branches. (b) Calculated electronic contribution to the phonon line width 2γ for the LO1 and LO2 branches with two numerical smearing parameters: $\sigma = 0.1$ and 1.0 eV.

particular, the minimum in the dispersion of the LO1 mode is observed. As discussed in Sec. IV A, the concurrence of the dip in the dispersion of the LO1 branch and the maximum of the dispersion of the soft mode at $h = 0.2$–0.25 r.l.u. might suggest an exchange of eigenvectors between the two modes at these wave vectors. However, the dispersion of the LO1 branch does not change between $T = 33$ and 250 K. This is in contrast to the huge temperature effect in the acoustic mode and speaks against a sizable interaction of the branches, in agreement with our theoretical analysis of the line width contributions.

To investigate a possible interaction of the optic and acoustic modes more closely, we measured the soft mode energies going radially away from $\mathbf{q}_{CDW}$ in various directions in reciprocal space [Fig. 5(a)]. We found that the dispersions can be well approximated by a straight line regardless of whether we move away from $\mathbf{q}_{CDW}$ within the basal plane or along the (001) direction. Results for the latter direction demonstrate that the softening occurs only in a small region of reciprocal space. In our experimental setup, consecutive analyzers of the HERIX spectrometer sampled different wave vectors, which were spaced along the (h,0,l) line in reciprocal space. Hence, we are able to construct a two-dimensional dispersion surface of the LO1 branch in the (h,0,l) plane. For simplicity, we show the results as line scans for different values of $0 \leqslant l \leqslant 0.27$ [Fig. 5(b)]. Apparently, the dispersion does not depend on l. The qualitative discrepancy between the l dependence of the soft mode and the LO1 branch further indicates that an interaction between the two branches is small or absent. These observations are in excellent agreement with DFPT, which predicts a 4-meV higher energy of the soft mode at $\mathbf{q} = \mathbf{q}_{CDW} + (0,0,0.5)$ [corresponds to $|\mathbf{q} - \mathbf{q}_{CDW}| \approx 0.25$ Å^{-1} in Fig. 5(a)]. Furthermore, the LO1 branch shows no l dependence in DFPT.

In Fig. 6(a), we plot the phonon line widths along the $\Gamma - M$ direction of the optic phonons at $T = 33$ and 250 K. In phonon spectra taken at $\mathbf{q} = (h,0,0)$, $h \leqslant 0.1$, the LO2 mode dominates, whereas for $h > 0.1$, the LO1 mode shows the larger spectral weight [e.g., see Fig. 4(a) for $h = 0.2$]. Though the determination of the phonon energies was almost always possible for both phonons, the line widths could only be measured accurately for the dominant peaks. Therefore, we show line widths in Fig. 6(a) for the LO2 modes at $h \leqslant 0.1$ and for the LO1 modes at $h \geqslant 0.15$.

We observe a nearly constant line width of $\sim$1 meV at $T = 250$ K, which we assign to the general imperfections of the crystal and anharmonic effects. At low temperatures, however, the line widths at wave vectors with $h \leqslant 0.2$ increase

significantly, whereas for $h \geqslant 0.25$ we find the same values as for high temperatures.

Here, we compare our results to calculations of the electronic contribution to the phonon line width 2γ in our DFPT calculation. Although DFPT is a zero-temperature technique, it was shown in several publications that the necessary numerical smearing of the electronic states σ acts like a thermal smearing in electronic momentum space and hence can be used to qualitatively simulate temperature effects.[26] Though temperatures equivalent to σ are at least one order of magnitude too large, our previous investigation of the soft mode in $2H$-$NbSe_2$ indicated that values of 0.1 eV $\leqslant \sigma \leqslant$ 1.0 eV produce results that are consistent with a temperature range of 30 K $\leqslant T \leqslant$ 300 K.[13]

Fig. 6(b) shows the calculated values of 2γ (corresponding to the FWHM) for the LO1 and LO2 phonon modes at the wave vectors corresponding to Fig. 6(a). We see good agreement regarding the wave vector dependence between the line widths at low temperature and 2γ calculated with $\sigma = 0.1$ eV, although the decrease of 2γ is somewhat more gradual than in the observed line width. This wave vector dependence is much reduced at $T = 250$ K, as well as in the calculations using $\sigma = 1.0$ eV. In particular, the calculations nicely reproduce the observed temperature effect at low values of h. Therefore, we assign this observation to the presence of EPC in these branches at $h \leqslant 0.2$.

In summary, the experimental results confirm the prediction of substantial EPC in optic phonon branches at small reduced wave vectors. The results of the phonon energies at different temperatures and away from the (1,0,0) high symmetry line do not indicate a strong interaction between the LO1 and the LA branches, in agreement with DFPT.

V. DISCUSSION

CDW order is only stabilized through a coupling to the lattice (EPC)[27] and hence, the investigation of the lattice degrees of freedom is a source of unique information in compounds undergoing a CDW phase transition. Theoretically, CDW materials were investigated intensively in the 1970s[7,27,28] and early 1980s[8] and, more recently, using modern *ab initio* methods.[22,29]

One important piece of information is the bare phonon energy $\omega_{\text{bare}}(q)$ in the absence of renormalization effects linked to the CDW phase transition. $\omega_{\text{bare}}(q)$ and the experimentally observable renormalized phonon frequency $\omega_q(q)$ are linked by[27]

$$\omega_q^2 = \omega_{\text{bare}}^2 - \frac{2N^3 g_q^2 Re\{\chi_q\}}{M[1 + (2\bar{U}_q - \bar{V}_q)Re\{\chi_q\}]} \tag{2}$$

where $N, M, \bar{U}_q$, and $\bar{V}_q$ are the Avogadro constant, ionic mass, average coulomb, and exchange matrix elements, respectively. In addition, χ_q is the electronic response function, and g_q is the EPC matrix element. Typically, the last term in Eq. (2) is small. In CDW compounds, it is expected that χ_q becomes large at $\mathbf{q}_{\text{CDW}}$, causing the collapse of the phonon mode. However, we showed in a recent publication,[13] for the case of $2H$-$NbSe_2$, that the wave vector dependence of the EPC matrix element g_q can lead to a CDW instability.

For better understanding, it is instructive to explain the bare phonon energy ω_{bare} in more detail. The originally very high phonon energies of the lattice of ionic nuclei are reduced to the typical values in the millielectron volt range by the general screening of all electrons in a solid. Our interest lies in the additional screening due to the presence of the CDW phase transition. These processes involve primarily the bands forming the Fermi surface. Therefore, we consider in our analysis only the contributions of the three bands crossing E_F to the electronic susceptibility $\chi_{q,FS}$, the real part of which was calculated, e.g., by Johannes *et al.*[24] Accordingly, ω_{bare} can be related to the observed energy ω_q by Eq. (2) if we replace $Re\chi_q$ with $Re\chi_{q,\text{FS}}$. The $\mathbf{q}$ dependence of the difference between ω_q^2 and ω_{bare}^2 is governed by $Re\chi_{q,\text{FS}}$, g_q, or both, where g_q is the EPC matrix element involving the respective phonons and electronic scattering processes. In a previous publication,[13] we argued that, in the case of $2H$-$NbSe_2$, it is the latter, which determines the soft mode dispersion and defines the periodicity of the ordered phase, i.e., $\mathbf{q}_{\text{CDW}}$. This point of view is corroborated by the results presented in this publication.

In Sec. IV, we showed that an exchange of eigenvectors between LO and LA phonons with Σ_1 symmetry is unlikely; hence, an acousticlike assumption for the bare phonon dispersion $\omega_{\text{bare}}(q)$ is justified for $NbSe_2$.

Before we can apply Eq. (2) in order to estimate $\omega_{\text{bare}}(q)$, we need to take into account that the $\mathbf{q}$ dependence of γ is largely due to scattering between the two Nb bands at the Fermi surface and that the strong wave vector dependence of γ can originate in the corresponding EPC matrix element, electronic joint density of states (JDOS), or both.[30] The JDOS varies only by $\pm 15\%$ along $\Gamma - M$ (not shown). Thus, the matrix elements for the Nb_1 – Nb_2 interband scattering exhibit the strong wave vector dependence. This is in good agreement with experiments using angle-resolved photoemission spectroscopy (ARPES), which reported the highest EPC strength on the double-walled Nb $4d$-derived Fermi surface sheet.[31]

Therefore, we can extract in a first approximation the wave vector dependence of the EPC matrix element from our measurements and apply this knowledge in Eq. (2). The approximation originates in γ being proportional to the square of the momentum-averaged EPC matrix element $|\overline{g_q}|^2$,[30]

$$\gamma_q \propto |\overline{g_q}|^2 \times \text{JDOS}. \tag{3}$$

However, $\overline{g_q}$ should in general have a weaker wave vector dependence than g_q, i.e., we expect to underestimate the real wave vector dependence of g_q. Concerning our discussion of which electrons should be taken into account in order to analyze the renormalization at the CDW phase transition, we use the wave vector dependence of $Re\chi_{q,\text{FS}}$, as calculated by Johannes *et al.*,[24] where only contributions from the three electronic bands crossing the Fermi energy were taken into account. It is also in good agreement with estimates based on ARPES experiments.[32]

Fig. 7 displays our analysis of the renormalized and bare phonon dispersions based on Eq. (2) in comparison to the experimental energies at $T = 33$ and 250 K. We use Eq. (2) in a parameterized form,

$$\omega_q^2 = \omega_{\text{bare}}^2(h) - \frac{c_1 \times f_g(h)}{\left(\frac{1}{Re\chi_{q,\text{FS}}(h)} + c_2\right)} \tag{4}$$

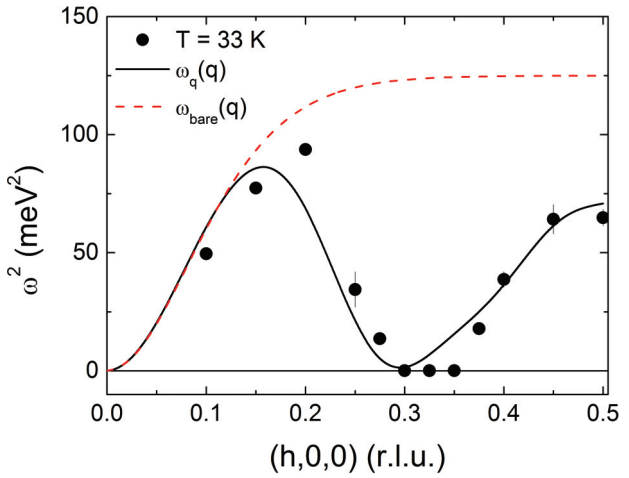

FIG. 7. (Color online) (a) Fit (solid line) of the observed square soft mode energies at $T = T_{CDW}$ (dots) using Eq. (3) and $Re\chi_{q,FS}(h)$ and $g_q(h)$ as extracted from DFPT. ω_{bare} (dashed line) was approximated by a Brillouin function with two fit parameters.

where ω_{bare} was approximated by a Brillouin function with two parameters.[33] $f_g(h)$ and $Re\chi_{q,FS}(h)$ are the wave vector dependences of g_q^2 and $Re\chi_q$, respectively. The latter was taken from Ref. 24 [Fig. 7]. For $f_g(h)$, we used the functional form of the contribution to γ calculated for the acoustic mode, which is due to scattering between the two Nb 4d-derived bands at the Fermi surface [red dots in Fig. 2(f)]. The fit was constraint by $c_2 = 2\bar{U}_q - \bar{V}_q$ having a positive value. It turned out to be a very small number, the exact absolute value having negligible influence on the resulting bare dispersion, in agreement with assumptions in Ref. 27. The parameter c_1 takes care of the prefactors given in Eq. (2), and the wave vector-dependent function $f_g(h)$ is only proportional to the EPC matrix element g_q^2 (see above).

Results of our analysis shown in Fig. 7 demonstrate that the renormalized phonon dispersion at $T = T_{CDW}$ can be well described based on an acoustic bare phonon dispersion with a zone boundary energy of 11.2 meV. The fitted bare dispersion is in reasonable agreement with phonon energies measured near room temperature, although the dispersion at $T = 250$ K is still renormalized, which is evident in the clearly observable dip around $\mathbf{q}_{CDW}$.[13] Our analysis of the phonons in $NbSe_2$ based on lattice dynamical calculations using DFPT yields a sensible bare phonon dispersion, which is further evidence for the accuracy of the model and proposed point of view in Ref. 13 that the wave vector dependence of the EPC drives the CDW transition in this compound. This was recently corroborated by results from scanning tunneling microscopy (STM).[34] Apart from the usually observed triple-$\mathbf{q}$ CDW vector $\mathbf{q}_{CDW} = (0.329,0,0)$, STM revealed surface regions with a unidirectional CDW vector $\mathbf{q}_{1Q} \approx (2/7,0,0)$. The minimum of the fitted soft mode dispersion at $T = T_{CDW}$ is close to the value of $h = 2/7$. However, we do not see a clear link between our results and the single-$\mathbf{q}$ CDW order observed by STM.[34] Experimentally, inelastic x-ray scattering is a bulk probe, and the DFPT calculations even overestimate the position of the CDW vector along the $\Gamma - M$ direction, with the dispersion minimum at $\mathbf{q} = (0.375,0,0)$ [Fig. 1(a), see also Fig. 4 in Ref. 13 for more details].

VI. CONCLUSION

We have reported an inelastic x-ray scattering and *ab initio* theoretical investigation of the lattice dynamics of $NbSe_2$, focusing on longitudinal phonon modes across the CDW-ordering wave vector $\mathbf{q}_{CDW} = (0.329,0,0)$, i.e., in the (100) direction. We derive an acousticlike bare dispersion $\omega_{bare}(q)$ of the CDW soft phonon mode from the wave vector dependence of the EPC matrix element g_q and the response of the electrons forming the Fermi surface. Although our measurements provide evidence for EPC in optic branches as well, we demonstrate that there is no significant intermode hybridization. Furthermore, our analysis shows that the observed wave vector-dependent EPC originates from one particular electronic scattering process between two Nb – 4d-derived bands at the Fermi surface. Together with a corresponding quasiconstant electronic JDOS for these scattering processes, this is evidence of the strong wave vector dependence of the EPC matrix elements.

ACKNOWLEDGMENTS

We acknowledge discussions with J. van Wezel. We thank John M. Tranquada for supplying us with a single crystal of 2H-$NbSe_2$. F.W. was supported by the young investigator group "Competing phases in superconducting materials" of the Helmholtz Society (VH-NG-840). D.R. was supported by the US Department of Energy (DOE), Office of Science, Office of Basic Energy Sciences, under Contract No. DE-SC0006939. Work at Argonne was supported by US DOE, Office of Science, Office of Basic Energy Sciences, under Contract No. DE-AC02-06CH11357.

[1] S. A. Kivelson, I. P. Bindloss, E. Fradkin, V. Oganesyan, J. M. Tranquada, A. Kapitulnik, and C. Howald, Rev. Mod. Phys. **75**, 1201 (2003).
[2] E. Dagotto, Science **309**, 257 (2005).
[3] E. Revolinsky, G. A. Spiering, and D. J. Beerntsen, J. Phys. Chem. Solid. **26**, 1029 (1965).
[4] J. A. Wilson, F. J. D. Salvo, and S. Mahajan, Adv. Phys. **24**, 117 (1975).
[5] C. D. Malliakas and M. G. Kanatzidis, J. Am. Chem. Soc. **135**, 1719 (2013).
[6] H. Smith and W. Gläser, Phys. Rev. Lett. **25**, 1611 (1970).
[7] N. J. Doran, J. Phys. C **11**, L959 (1978); W. Weber, Phys. Rev. B **8**, 5082 (1973).
[8] C. M. Varma and A. L. Simons, Phys. Rev. Lett. **51**, 138 (1983).
[9] S. Sinha and B. Harmon, Phys. Rev. Lett. **35**, 1515 (1975).
[10] D. E. Moncton, J. D. Axe, and F. J. DiSalvo, Phys. Rev. B **16**, 801 (1977).
[11] C. Ayache, R. Currat, B. Hennion, and P. Molinie, J. Phys. IV **3**, 125 (1993).

[12]K. Schmalzl, D. Strauch, A. Hiess, and H. Berger, J. Phys. Condens. Matter **20**, 104240 (2008).
[13]F. Weber, S. Rosenkranz, J. P. Castellan, R. Osborn, R. Hott, R. Heid, K. P. Bohnen, T. Egami, A. H. Said, and D. Reznik, Phys. Rev. Lett. **107**, 107403 (2011).
[14]B. Meyer, C. Elsässer, F. Lechermann, and M. Fähnle, FORTRAN90, Program for Mixed-Basis-Pseudopotential Calculations for Crystals, Max-Planck-Institut für Metallforschung, Stuttgart.
[15]S. Baroni, S. de Gironcoli, A. Dal Corso, and P. Giannozzi, Rev. Mod. Phys. **73**, 515 (2001).
[16]R. Heid and K.-P. Bohnen, Phys. Rev. B **60**, R3709 (1999).
[17]T. S. Toellner, A. Alatas, and A. H. Said, J. Synchrotron Rad. **18**, 605 (2011).
[18]A. H. Said, H. Sinn, and R. Divan, J. Synchrotron Rad. **18**, 492 (2011).
[19]D. E. Moncton, J. D. Axe, and F. J. DiSalvo, Phys. Rev. Lett. **34**, 734 (1975).
[20]B. Fåk and B. Dorner, Phys. B **234-236**, 1107 (1997).
[21]G. Shirane, S. Shapiro, and J. Tranquada, *Neutron Scattering with a Triple-Axis Spectrometer* (Cambridge University Press, Cambridge, UK, 2002).
[22]M. Calandra, I. I. Mazin, and F. Mauri, Phys. Rev. B **80**, 241108 (2009).
[23]K. Rossnagel, O. Seifarth, L. Kipp, M. Skibowski, D. Voß, P. Krüger, A. Mazur, and J. Pollmann, Phys. Rev. B **64**, 235119 (2001).
[24]M. D. Johannes, I. I. Mazin, and C. A. Howells, Phys. Rev. B **73**, 205102 (2006).
[25]B. Renker, H. Rietschel, L. Pintschovius, W. Gläser, P. Brüesch, D. Kuse, and M. J. Rice, Phys. Rev. Lett. **30**, 1144 (1973); J. P. Pouget, B. Hennion, C. Escribe-Filippini, and M. Sato, Phys. Rev. B **43**, 8421 (1991).
[26]K.-P. Bohnen, R. Heid, H. J. Liu, and C. T. Chan, Phys. Rev. Lett. **93**, 245501 (2004); L. Pintschovius, F. Weber, W. Reichardt, A. Kreyssig, R. Heid, D. Reznik, O. Stockert, and K. Hradil, Pramana **71**, 687 (2008).
[27]S. K. Chan and V. Heine, J. Phys. F **3**, 795 (1973).
[28]N. J. Doran, B. Ricco, M. Schreiber, D. Titterington, and G. Wexler, J. Phys. C **11**, 699 (1978).
[29]M. Calandra and F. Mauri, Phys. Rev. Lett. **106**, 196406 (2011).
[30]R. Heid, K.-P. Bohnen, and Renker, Adv. Solid State Phys. **42**, 293 (2002).
[31]D. J. Rahn, S. Hellmann, M. Kalläne, C. Sohrt, T. K. Kim, L. Kipp, and K. Rossnagel, Phys. Rev. B **85**, 224532 (2012).
[32]D. S. Inosov, V. B. Zabolotnyy, D. Evtushinsky, A. Kordyuk, B. Buechner, R. Follath, H. Berger, and S. Borisenko, New J. Phys. **10**, 125027 (2008).
[33]It can be easily shown that a Brillouin function gives a better description of a typical acoustic dispersion than does the simpler sine function.
[34]A. Soumyanarayanan, M. M. Yee, Y. He, J. van Wezel, D. J. Rahn, K. Rossnagel, E. W. Hudson, M. R. Norman, and J. E. Hoffman, Proc. Natl. Acad. Sci. USA **110**, 1623 (2013).